

The structural and scaling properties of nearby galaxy clusters - II. The $M-T$ relation

M. Arnaud¹, E. Pointecouteau¹ and G.W. Pratt²

¹ CEA/DSM/DAPNIA Service d'Astrophysique, C.E. Saclay, L'Orme des Merisiers, Bat. 709, F-91191 Gif sur Yvette, France

² MPE, Giessenbachstraße, 85748 Garching, Germany

Received: February 10, 2005; accepted

Abstract. Using a sample of ten nearby ($z \lesssim 0.15$), relaxed galaxy clusters in the temperature range [2 – 9] keV, we have investigated the scaling relation between the mass at various density contrasts ($\delta = 2500, 1000, 500, 200$) and the cluster temperature. The masses are derived from precise mass profiles measured with *XMM-Newton* at least down to $\delta = 1000$ and well described by a NFW type model. The logarithmic slope of the $M-T$ relation is well constrained and is the same at all δ , reflecting the self-similarity of the mass profiles. At $\delta = 500$, the slope of the relation for the sub-sample of hot clusters ($kT > 3.5$ keV) is consistent with the standard self-similar expectation: $\alpha = 1.49 \pm 0.15$. The relation steepens when the whole sample is considered: $\alpha = 1.71 \pm 0.09$. The normalisation of the relation is discrepant (by $\sim 30\%$), at all density contrasts, with the prediction from purely gravitation based models. Models that take into account radiative cooling and galaxy feedback are generally in better agreement with our data. We argue that remaining discrepancies, in particular at low δ , are more likely due to problems with models of the ICM thermal structure rather than to an incorrect estimate of the mass from X-ray data.

Key words. Cosmology: observations matter, Cosmology: dark matter, Galaxies: cluster: general, (Galaxies) Intergalactic medium, X-rays: galaxies: clusters

1. Introduction

From a theoretical point of view, galaxy clusters are characterised by their mass. Models of structure formation predict the space density, spatial distribution and physical properties of clusters (internal structure, radius, temperature, luminosity, etc) as a function of mass and redshift (see Bertschinger 1998, for a review). However, observationally, the mass is not easily measured, and the observed scaling relations are in fact expressed in terms of the temperature T , rather than the mass M . These scaling relations are important sources of information on the physics of cluster formation (e.g. Voit & Ponman 2003). For the information to be complete, we must determine the $M-T$ relation itself, which provides the missing link between the gas properties and the mass. Furthermore, measures of the cosmological parameters, such as σ_8 , Ω_m and w , from cluster abundance or spatial distribution, rely heavily on this relation to link the mass to the X-ray observables available from X-ray cluster surveys. The present error on the value of σ_8 , as determined from X-ray observations, is dominated by uncertainty on the $M-T$ relation (Pierpaoli et al. 2003; Viana et al. 2003; Henry 2004), and a precise calibration of this relation is mandatory if we want to do precise cosmology with clusters (Borgani 2003).

The average temperature is expected to be closely related to the mass, via the virial theorem. We can first define M_δ as the mass within the radius R_δ , inside which the mean mass density is δ times the critical density, $\rho_c(z) = 3h(z)^2H_0/8\pi G$, at the cluster redshift. We then expect $h(z)M_\delta = A(\delta)T^{3/2}$, if clusters are in hydrostatic equilibrium and they obey self-similarity. Here $h(z)$ is the Hubble constant normalised to its local value and $A(\delta)$ depends on the internal structure. The above relation is remarkably well verified by adiabatic numerical simulations, down to $\delta \sim 200$, which roughly corresponds to the virialised part of clusters (e.g. Evrard & Gioia 2002).

For relaxed clusters, the mass can be derived from X-ray observations of the gas density and temperature profile and the hydrostatic equilibrium equation. In recent years, a sustained observational effort to measure the local $M-T$ relation has been undertaken using *ROSAT*, *ASCA* and *BeppoSAX*, but no definitive picture has yet emerged. It is unclear whether the mass scales as $T^{3/2}$ as expected (Horner et al. 1999; Ettori et al. 2002; Castillo-Morales & Schindler 2003); or if this is true only in the high mass regime ($kT \gtrsim 4$ keV), with a steepening at lower mass (Nevalainen et al. 2000; Xu et al. 2001; Finoguenov et al. 2001); or even if the slope is higher over the entire mass range (Sanderson et al. 2003). The derived normalisations of the $M-T$ relation derived from *ASCA* data are generally lower than predicted by adiabatic numerical simulations (e.g. Nevalainen et al. 2000; Finoguenov et al. 2001), typically 40% below the prediction of Evrard et al. (1996). On the other

Send offprint requests to: M. Arnaud, e-mail:
marnaud@discovery.saclay.cea.fr

hand, using *BeppoSAX* data, Ettori et al. (2002) found a normalisation consistent with the predictions (although the errors were large).

These studies had to rely largely on extrapolation to derive the virial mass, and were limited by the low resolution and statistical quality of the temperature profiles. With *XMM-Newton* and *Chandra* we can now measure the mass profile of clusters with unprecedented accuracy. Using *Chandra* observations, Allen et al. (2001) derived an $M-T$ relation slope of 1.51 ± 0.27 (consistent with the self-similar model), and, confirmed the offset in normalisation. However, their sample comprised only 5 hot (i.e. massive) clusters ($kT > 5.5$ keV), and, due to relatively small *Chandra* field of view, their $M-T$ relation was established at R_{2500} (i.e. about $\sim 0.3R_{200}$).

In a recent paper (Pointecouteau et al. 2005, hereafter, Paper I), we measured the integrated mass profiles of ten relaxed, nearby clusters observed with *XMM-Newton*. The sample has an excellent temperature coverage, from 2 to 9 keV. The mass profiles cover a wide range of radii (from $0.01R_{200}$ to $0.7R_{200}$), and are particularly well constrained between $0.1R_{200}$ and $0.5R_{200}$. In Paper I, we studied the structural properties of the mass profiles, in order to test current scenarios for the Dark Matter clustering. In this paper, the data are used to establish a precise $M-T$ relation up to the virial radius. In Sect. 2, we describe how we derive the temperature and mass data. In Sect. 3 we present and compare the $M-T$ relations at various density contrasts. We discuss the reliability of the X-ray mass estimates in Sect. 4. The derived $M-T$ relations are discussed with respect to pre-*Chandra/XMM-Newton* results in Sect. 5 and with expectations from models in Sect. 6. Our conclusions are presented in Sect. 7.

Throughout the paper, results are given for the currently-favoured Λ CDM cosmology, with $H_0 = 70$ km/s/Mpc, $\Omega_m = 0.3$ and $\Omega_\Lambda = 0.7$.

2. The data

2.1. The mass at various density contrasts

We used the mass profiles determined in Paper I to estimate the mass at four density contrasts: $\delta = 2500, 1000, 500$ and 200 ¹. We recall that the mass profiles were derived from the observed density and temperature profiles (corrected for PSF and projection effects) using the hydrostatic equilibrium equation. The mass and errors at each radius of the temperature profile were calculated using a Monte Carlo method.

In Paper I, we found that the mass profiles are well described by an NFW-type model (Navarro et al. 1997):

$$M_{\text{NFW}}(r) = M_{200} \frac{\ln(1 + c_{200}x) - c_{200}x/(1 + c_{200}x)}{\ln(1 + c_{200}) - c_{200}/(1 + c_{200})}, \quad (1)$$

where $x = r/R_{200}$. The concentration c_{200} , and the mass M_{200} , are free parameters determined by the fitting procedure. R_{200}

¹ We chose these δ s for the following reasons. $\delta = 2500$ allows a direct comparison with previous *Chandra* results. $\delta = 1000$ is the density contrast limit of our observations. $\delta = 500$ corresponds to the edge of the virialized part of clusters in a conservative approach. $\delta = 200$ is the classical 'virial' radius in an $\Omega = 1$ universe.

is related to M_{200} via $M_{200}/R_{200}^3 = (4\pi/3)200\rho_c(z)$. The best fitting M_{200} and R_{200} values are recalled in Table 1. We can equivalently fit the data using the mass at any other density contrast as a free parameter, and by doing so, we can directly estimate the error on each M_δ . The resulting M_{2500} , M_{1000} and M_{500} values are also shown in Table 1. We also list the outermost radius (in units of R_{200}), and the corresponding density contrast δ_{obs} , reached by the temperature profiles (and thus the outermost extent of the mass profiles).

We will use these mass estimates to study the $M_\delta-T$ relation at various density contrasts. Our study is thus based on a parametric model of the observed mass profiles, rather than directly on the measured mass data. Let us discuss this point in more detail. All of the clusters are observed down to at least $\delta = 1000$ ($R_{1000} = (0.47 \pm 0.02)R_{200}$, averaged over the whole sample), the only exceptions being A1983 and MKW9 ($\delta_{\text{obs}} \sim 1400$). Using the best fitting model rather than the data is simply equivalent to 'smoothing' the data. We checked that this does not introduce a bias in the following way. For each cluster, we interpolated the observed profile expressed as a function of density contrast² in the log-log plane to estimate directly the mass at $\delta = 2500$, and compared this value to that derived from the NFW fit to the mass profile. In all cases the values are consistent within their 1σ errors. The ratio of the two values has a median value of 0.99 across the sample, and there is no significant correlation with mass. This reflects the fact that the NFW model is a good fit to the data, particularly in the $0.1R_{200} - 0.5R_{200}$ range (see Paper I).

As explained above, the estimates of M_{2500} and M_{1000} are made (almost) without data extrapolation. However, the mass estimates at $\delta = 500$ and $\delta = 200$ do involve extrapolation of the data. The M_{500} and M_{200} estimates rely on the assumption that the best fitting NFW model remains a good representation of the cluster mass profile beyond δ_{obs} . We further discuss the reliability of this assumption in Sect. 4.

2.2. Overall temperature

To investigate the $M - T$ relation, we need to define a global temperature. For this quantity, we used the overall spectroscopic temperature of the $0.1R_{200} \leq r \leq 0.5R_{200}$ region. The lower boundary of $0.1 R_{200}$ was chosen so as to avoid most of the cooling core, where a large dispersion is observed in the temperature profiles (Fig. 1). The upper boundary is limited by the quality of the spectroscopic data. An upper boundary of $0.5 R_{200}$ appeared a good compromise. Only the data from A1983 and MKW9 do not quite reach this radius; they are however detected up to $\sim 0.4 R_{200}$ (see Table 1). Note that $0.5 R_{200}$ corresponds roughly to $\delta = 1000$.

For each cluster, we performed an isothermal fit of the spectrum extracted within the $[0.1 - 0.5]R_{200}$ range, R_{200} being derived from the best fitting NFW model (see above). In the fit, the abundance was let free and the N_{H} was fixed to the 21 cm value (except for A478, see Pointecouteau et al. (2004)). We corrected the derived value for PSF blurring and projection effects using the ratio of the mean emission-measure weighted

² $M(\delta)$ is readily derived from $M(r)$, using $\delta = 3M(r)/4\pi\rho_c(z)r^3$.

Table 1. Physical cluster parameters. Masses are in units of $10^{14} M_{\odot}$, and are given for a Λ CDM cosmology with $\Omega_m = 0.3$, $\Omega_{\Lambda} = 0.7$, $H_0 = 70$ km/s/Mpc. Errors are 1σ errors.

Cluster	z	kT (keV)	R_{200} (kpc)	M_{2500}	M_{1000}	M_{500}	M_{200}	R_{obs}/R_{200}	δ_{obs}
A1983	0.0442	2.18 ± 0.09	1103 ± 136	0.43 ± 0.09	0.77 ± 0.22	1.09 ± 0.37	1.59 ± 0.61	0.38	1455
MKW9	0.0498	2.43 ± 0.24	1006 ± 84	0.41 ± 0.07	0.66 ± 0.14	0.88 ± 0.20	1.20 ± 0.30	0.41	1401
A2717	0.0382	2.56 ± 0.06	1096 ± 44	0.45 ± 0.04	0.79 ± 0.08	1.10 ± 0.12	1.57 ± 0.19	0.54	727
A1991	0.0586	2.71 ± 0.07	1106 ± 41	0.58 ± 0.05	0.91 ± 0.09	1.20 ± 0.12	1.63 ± 0.18	0.60	655
A2597	0.0852	3.67 ± 0.09	1344 ± 49	1.08 ± 0.07	1.69 ± 0.14	2.22 ± 0.22	3.00 ± 0.33	0.57	713
A1068	0.1375	4.67 ± 0.11	1635 ± 47	1.47 ± 0.07	2.69 ± 0.16	3.87 ± 0.28	5.68 ± 0.49	0.58	622
A1413	0.1430	6.62 ± 0.14	1707 ± 57	2.33 ± 0.13	3.66 ± 0.27	4.82 ± 0.42	6.50 ± 0.65	0.79	339
A478	0.0881	7.05 ± 0.12	2060 ± 112	3.12 ± 0.31	5.43 ± 0.70	7.57 ± 1.11	10.8 ± 1.8	0.58	650
PKS 0745-191	0.1028	7.97 ± 0.28	1999 ± 77	3.32 ± 0.23	5.41 ± 0.49	7.27 ± 0.75	10.0 ± 1.2	0.57	694
A2204	0.1523	8.26 ± 0.22	2075 ± 77	3.62 ± 0.22	6.11 ± 0.51	8.39 ± 0.81	11.8 ± 1.3	0.61	580

Columns: (1) Cluster name; (2) Redshift; (3) Spectroscopic temperature of the $0.1 < r < 0.5 R_{200}$ region; (4) R_{200} , roughly the virial radius in numerical simulations; (5,6,7,8) Total mass at density contrast $\delta = 2500, 1000, 500, 200$, derived from an NFW fit to the observed mass profile; (9) Fraction of R_{200} spectroscopically observed (outer radius of the final temperature bin); (10) Corresponding density contrast.

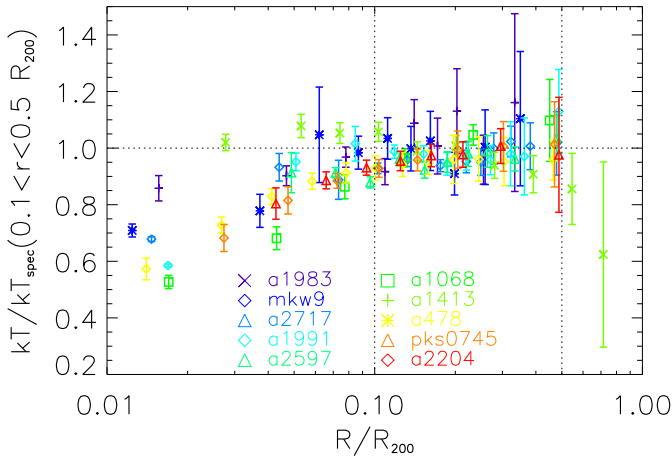


Fig. 1. Temperature profiles. The temperatures have been normalised to the spectroscopic temperature measured in $0.1 < r < 0.5 R_{200}$ region; the radius has been scaled to R_{200} . The profiles have been corrected for PSF and projection effects (see Paper I for details).

value of the temperature profile in the $[0.1 - 0.5] R_{200}$ region after PSF/projection correction to the mean value before correction (see Paper I for details on the correction procedure). The correction factor is generally negligible and is always less than 5%. The resulting temperature values are given in Table 1.

We could have estimated a 'mass-weighted' temperature in the $0.1R_{200} < r < 0.5R_{200}$ region from the temperature profile. However, this temperature would still be a 'spectroscopic' temperature since it would be derived from averaging over measured X-ray temperatures. It would not, strictly speaking, be equivalent to the 'mass-weighted' temperature derived from numerical simulations. We thus preferred to use the overall spectroscopic temperature, which is a directly measured quantity and can also easily be estimated in numerical simulations. Since the region is defined in scaled radius, it can be derived from the simulated temperature profiles, using for instance the

approach proposed recently by Mazzotta et al. (2004). In addition, we note that only a global spectroscopic temperature can be usually estimated for high z clusters. In our approach, the extraction region can be similarly defined and our definition thus allows a consistent study of the evolution of the $M-T$ relation.

We note that Allen et al. (2001) use a mass-weighted temperature, T_{2500} , estimated from the temperature profile in the $r < R_{2500} \sim 0.3R_{200}$ region. In practice, their definition is equivalent to ours because i) the temperature profiles are fairly flat beyond the cooling core region ($r > 0.1R_{200}$) in both studies, and ii) the cooling core does not contribute much in mass to the average. This can be checked from Fig. 1 of Allen et al. (2001), where T_{2500} cannot be distinguished from the spectroscopic temperature of the plateau beyond the cooling core.

3. The $M - T$ relation

3.1. The $M_{2500} - T$ relation

In order to check the consistency of our *XMM-Newton* results with the *Chandra* study of Allen et al. (2001), we first investigated the $M_{2500} - T$ relation. For our sample, $\delta = 2500$ corresponds to an average radius of $[0.29 \pm 0.02] R_{200}$, where the mass is particularly well constrained for all clusters.

The sample studied by Allen et al. (2001) comprises hot lensing clusters (5.5 to 15 keV). We thus considered only the sub-sample of clusters with moderate to high temperatures (i.e. $T > 3.5$ keV), and fitted the $M_{2500}-T$ relation using a power law model of the form:

$$h(z)M_{\delta} = A_{\delta} \left[\frac{kT}{5 \text{ keV}} \right]^{\alpha}. \quad (2)$$

Here and in the following, the fit is performed using linear regression in the log-log plane, and the goodness of fit is calculated using a χ^2 estimator taking into account the errors on both mass and temperature. Note that, as in the study of Allen et al. (2001), the masses are scaled by $h(z)$, which corrects for the evolution expected in the standard self-similar model. This scaling factor is small in our z range ($h(z) = 1.07$ at $z = 0.15$)

Table 2. Results of power law fits to the $M_\delta - T$ and $R_\delta - T$ relation at various density contrasts δ . The data are fitted with a power law of the form $h(z)M_\delta = A_\delta \times (kT/5 \text{ keV})^\alpha$ and $h(z)R_\delta = B_\delta \times (kT/5 \text{ keV})^\beta$, where kT is the overall spectroscopic temperature of the $[0.1R_{200} - 0.5R_{200}]$ region. A Λ CDM cosmology is assumed with $\Omega_m = 0.3$, $\Omega_\Lambda = 0.7$, $H_0 = 70 \text{ km/s/Mpc}$

δ	$M_\delta - T$ relation		$R_\delta - T$ relation		$\chi^2(\text{dof})$	nph
	$A_\delta (10^{14} M_\odot)$	α	$B_\delta (\text{kpc})$	β		
Whole sample						
200	5.34 ± 0.22	1.72 ± 0.10	1674 ± 23	0.57 ± 0.02	14.49(8)	0.07
500	3.84 ± 0.14	1.71 ± 0.09	1104 ± 13	0.57 ± 0.02	12.65(8)	0.12
1000	2.82 ± 0.09	1.71 ± 0.08	791 ± 8	0.57 ± 0.02	10.74(8)	0.22
2500	1.69 ± 0.05	1.70 ± 0.07	491 ± 4	0.56 ± 0.02	9.33(8)	0.32
$T > 3.5 \text{ keV}$						
200	5.74 ± 0.30	1.49 ± 0.17	1714 ± 30	0.50 ± 0.05	10.45(4)	0.03
500	4.10 ± 0.19	1.49 ± 0.15	1129 ± 17	0.50 ± 0.05	8.34(4)	0.08
1000	3.00 ± 0.12	1.49 ± 0.14	807 ± 10	0.50 ± 0.04	5.91(4)	0.21
2500	1.79 ± 0.06	1.51 ± 0.11	500 ± 5	0.50 ± 0.03	2.50(4)	0.65

Columns: (1) Density contrast δ ; (2, 3) Intercept and slope for the $M_\delta - T$ relation: $E(z)M_\delta = A_\delta \times (kT/5 \text{ keV})^\alpha$; (4, 5) Intercept and slope for the $R_\delta - T$ relation: $E(z)R_\delta = B_\delta \times (kT/5 \text{ keV})^\beta$; (6) Chi-squared and degree of freedom; (7) Null probability hypothesis associated with the best fit.

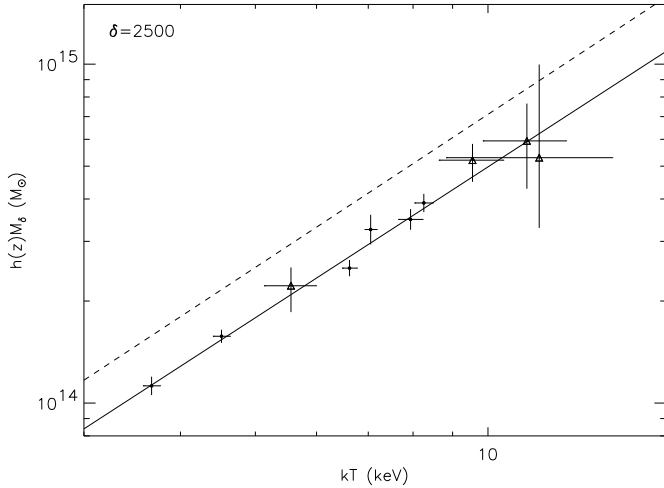


Fig. 2. The $M - T$ relation at $\delta = 2500$ as seen by *XMM-Newton* from the observation of 6 hot ($kT > 3.5 \text{ keV}$), relaxed clusters. Filled squares show the *XMM-Newton* data points; the full line shows the best fitting power law. The data on 4 published *Chandra* clusters (triangles) have been added to the fit but due to their large error bars, they do not change the parameters of the fit to the *XMM-Newton* data only (see text). The dashed black line is the prediction from adiabatic numerical simulations (Evrard et al. 1996).

but varies between ~ 1.05 and ~ 1.28 for the *Chandra* clusters located at higher redshifts ($0.1 < z < 0.46$).

The data are well fitted by a power law ($\chi^2/\text{dof} = 2.5/4$). The slope, $\alpha = 1.51 \pm 0.11$, is perfectly consistent with the expectation from the standard self-similar model, and with the results from *Chandra* observations ($\alpha = 1.51 \pm 0.27$). The derived normalisation, $A = (1.79 \pm 0.06) \times 10^{14} M_\odot$, is also consistent with the *Chandra* normalisation (see Table 3). As noted by Allen et al. (2001), such a normalisation is discrepant with the value derived from numerical simulations including gravita-

tional heating only: our measured value is about $\sim 30\%$ below the prediction of Evrard et al. (1996). When the *Chandra* data for 4 of the 5 clusters studied by Allen et al. (2001) are added to the present data set³, the best fitting values are almost unchanged ($\alpha = 1.52 \pm 0.1$ with the same intercept). This is due to the larger uncertainties in the *Chandra* temperature and mass determinations compared to those measured here (see Fig. 2). Figure 2 shows the best fit for the combined *XMM-Newton* and *Chandra* data compared to the expectations from the adiabatic numerical simulations of Evrard et al. (1996).

Still working at $\delta = 2500$, we performed a fit over the whole *XMM-Newton* sample, i.e. now including the four low mass systems. We obtain $\alpha = 1.70 \pm 0.07$, and a normalisation $A = (1.79 \pm 0.06) \times 10^{14} M_\odot$. The fit is acceptable, although formally less good ($\chi^2/\text{dof} = 9.33/8$). The slope now differs significantly from the expected value of $\alpha = 1.5$, and is just barely consistent with it at a 3σ level. This is further discussed in Sec. 6.2.

3.2. The $M_\delta - T$ relations up to the virial radius

Figure 3 shows the $M_\delta - T$ relations at various δ , together with the best fitting power law (Eq. 2) in each case, and the prediction from the numerical simulations of Evrard et al. (1996). The best fitting slopes and normalisations are listed in Table 2. The best fits are listed and plotted both for the whole sample, and for the sub-sample of hot clusters. The corresponding $R_\delta - T$ relations are also given in the Table.

The behaviour of the $M_{2500} - T$ relation is reproduced at all other density contrasts. The slope is stable on all spatial scales: the variation is at most 10% of the statistical error. It is always consistent with the expected $\alpha = 1.5$ value for the sub-sample of $T > 3.5 \text{ keV}$ clusters, whereas it steepens to $\alpha = 1.7$ when the cool clusters are included. Similarly, the normalisation re-

³ The fifth cluster is PKS 0745-191, which is common to both samples. We use only the *XMM-Newton* measurement for this analysis.

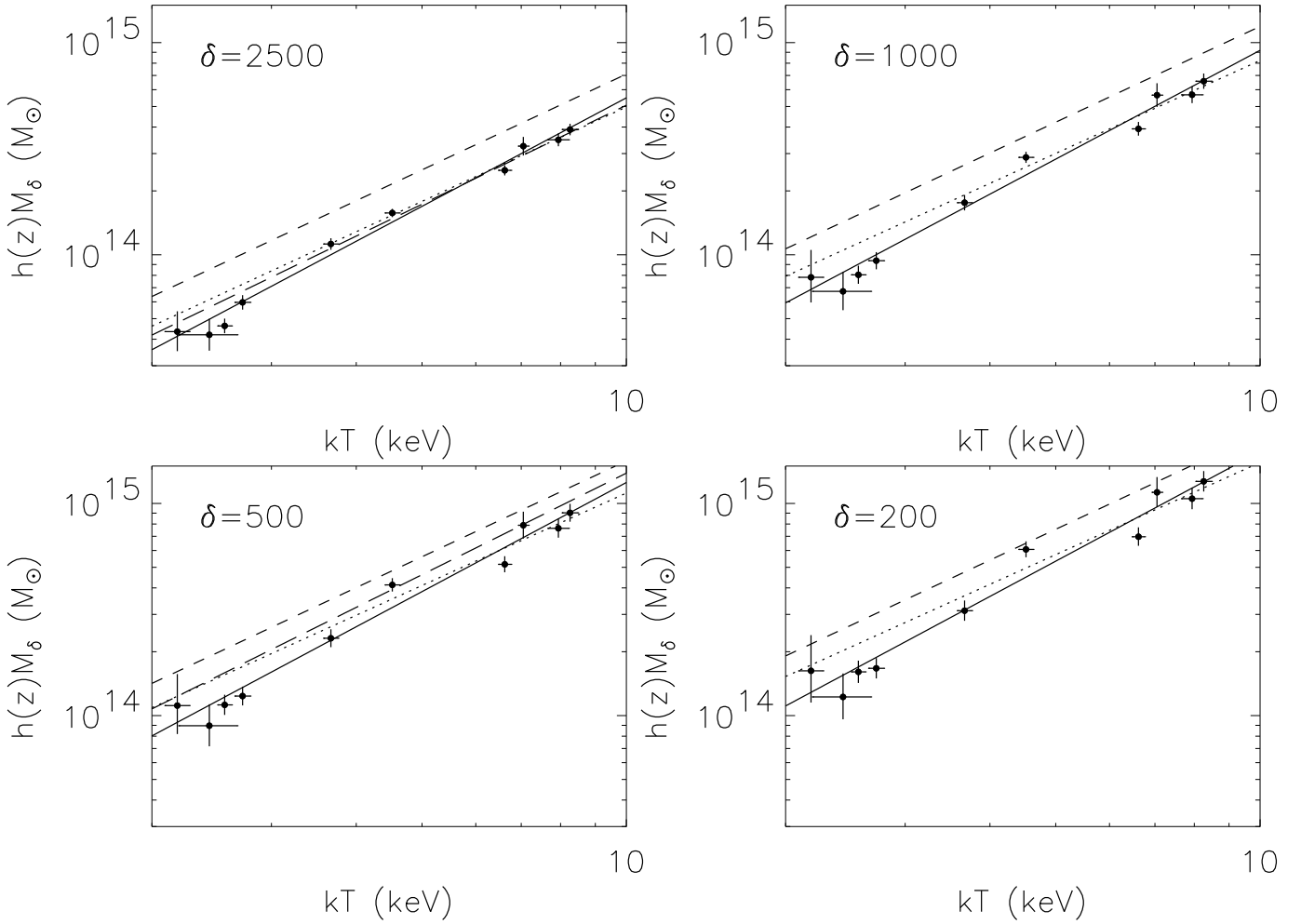


Fig. 3. The $M - T$ relation as seen by *XMM-Newton* from a sample of 10 clusters covering a temperature range from 2 to 9 keV. From top to bottom and left to right, the $M - T$ relation is given at the density contrasts δ of 200, 500, 1000 and 2500 with respect to the critical density of the Universe. Measurements are plotted with error bars. In each panel, the best fit for the whole sample is overplotted as a solid line, and the best fit for the hot cluster subsample is plotted as a dotted line. The predicted relation from adiabatic numerical simulations (Evrard et al. 1996) is overplotted as a dashed line. The long-dashed line (panels $\delta = 500$ and $\delta = 2500$) is the relation derived from a numerical simulation including radiative cooling, star formation and SN feedback (Borgani et al. 2004).

mains $\sim 30\%$ below the value from adiabatic numerical simulations of Evrard et al. (1996) at all δ .

This stable behavior is a direct consequence of the self-similarity of the mass profiles (Paper I). For an NFW type profile, the ratio of the masses at different density contrasts only depends on the concentration parameter, and $M_\delta = M_{2500}F(c, \delta)$. If all clusters had exactly the same concentration parameter (i.e., perfect self-similarity) the $M_\delta - T$ relations at various δ should only differ by their normalisation: $M_\delta = A(2500)F(c, \delta)T^\alpha$, for $M_{2500} = A(2500)T^\alpha$. The clusters in our sample are not perfectly self-similar but there is no significant variation of c with mass, and thus temperature (see Fig. 3 of Paper I). This explains the observed invariance of the slope. Furthermore, the observed concentration parameter is consistent with theoretical expectations (Paper I). As a consequence, the variation with δ of the normalisation, $A(\delta) = A(2500)F(c, \delta)$, follows expectations, and the offset ob-

served at $\delta = 2500$ remains the same at all δ (see also Fig 13 of Pratt & Arnaud 2002, and Fig. 4).

However, the quality of the power law fit decreases with decreasing δ , as shown by the increasing reduced χ^2 (see Table 2). This behaviour corresponds to a significant increase of the scatter in the observed $M_\delta - T$ relation (see Fig. 3). This increased scatter is probably largely an artifact. $\delta = 2500$ corresponds to the radius where the mass is best measured. In the NFW fit, M_{2500} is extremely well constrained by the data around $\delta = 2500$, quasi-independently of the shape parameter c . On the other hand, the concentration c , is very sensitive to the data at low radii, in particular in the cooling core region, where the mass profile is least well constrained, and where there could be systematic errors due to the PSF/projection correction. Thus, in practice, the errors on c and M_{2500} are largely independent and both contribute to the errors on the mass at low density contrast. This is particularly true beyond δ_{obs} , since $M_\delta = M_{2500}F(c, \delta)$.

The same is true for the scatter. As a result we expect, as observed, increasing statistical errors on M_δ as δ decreases, and a corresponding increase of the scatter in the M_δ - T relation (reflecting the scatter in c , see Fig. 3 of Paper I). The increase is larger than that expected purely from the increase of statistical errors due to intrinsic scatter in c and/or systematic errors on c .

4. Reliability of X-ray mass estimates

As discussed in Paper I, there is an excellent *quantitative* agreement in *shape* between the X-ray mass profiles used in this work and the profile predicted by numerical simulations. The observed scaled profiles are well-described by the quasi-universal cusped profile (NFW-type profile) now found in all CDM simulations, and have concentration parameters as expected for their mass. As concluded in Paper I, this suggests that the Dark Matter collapse is well understood, at least down to the cluster scale. In turn, this gives us confidence in the *XMM-Newton* mass estimates, not only in the observed radial range, but also where we have extrapolated beyond it (i.e. at $\delta < \delta_{\text{obs}} \sim 1000$). By using the best fitting NFW model to estimate M_{500} and M_{200} , we have implicitly assumed that this model remains valid beyond δ_{obs} (Sec. 2.1). It would be surprising if this were not the case since i) it is consistent with the theoretical predictions below δ_{obs} , and ii) in one case (A1413), we were even able to check the validity of the NFW profile down to $\delta < 500$.

Strictly speaking, the good agreement between the observed and predicted shape of the mass profiles does not mean that the *absolute* value of the X-ray mass is correct. It could be subject to systematic errors. However, this systematic error has to be the same within the statistical errors at all observed δ , whatever the cluster temperature, for the correct universal shape of the mass profile to be recovered.

One possible source of such systematic error is a departure from hydrostatic equilibrium (HE). The recent simulations of Kay et al. (2004a) suggest that the mass determined from the HE equation underestimates the true mass, due to residual gas motion. The effect is about the same at all radii up to $\delta = 500$. It is of the order of 15% for adiabatic models and of 10% for models including cooling and feedback, with typical variations of $\pm 5\%$. Such variations would not significantly change the shape of the X-ray mass profiles, taking into account our statistical errors. Thus the measured M_{2500} and M_{1000} values, and thus the corresponding normalisation of the M_{2500} - T and M_{1000} - T relations, could well be $\sim 10\% - 15\%$ too low. The offset would be the same for the M_{500} - T and M_{200} - T relations, since they are derived from 'extrapolation' of the NFW model. Note that this is probably an upper limit, since we focus on particularly relaxed clusters.

Another possible source of systematic error is that associated with calibration uncertainties. Possible errors are of the order of 10%. Since the mass derived from the HE equation scales as $M \propto T$, this would translate into a systematic error on the estimate of the 'real' mass of clusters. However that would not change the normalisation of the 'observed' M - T relation, since that depends only on the *shape* of the temperature profile.

Table 3. Comparison of the present results with M - T relations from the literature. α is the logarithmic slope of the relation and A is the normalisation at $kT = 5$ keV, in units of $10^{14} M_\odot$ for $H_0 = 70$ km/s/Mpc.

Reference ^a	A	α	Method ^b
$\delta = 2500$			
<u>Observation</u>			
Present work	1.69 ± 0.05	1.70 ± 0.07	$M_{\text{NFW}}, T > 2.0$ keV
Present work	1.79 ± 0.06	1.51 ± 0.11	$M_{\text{NFW}}, T > 3.5$ keV
ASF01	1.88 ± 0.34^c	1.51 ± 0.27	$M_{\text{NFW}}, T > 5.5$ keV
SPF03	1.2 ± 0.4^c	1.84 ± 0.14	$M_{\beta\gamma}, T > 5.5$ keV
<u>Theory</u>			
EMN96	2.5	1.5	T_{em} , adiabatic simul.
BMS04	1.73 ± 0.35	1.55 ± 0.05	$T_{\text{m}}, T > 2.0$ keV
KSA04	1.97 ± 0.03	1.54 ± 0.05	T_{m}
$\delta = 500$			
<u>Observation</u>			
Present work	3.84 ± 0.14	1.71 ± 0.09	$M_{\text{NFW}}, T > 2.0$ keV
Present work	4.10 ± 0.19	1.49 ± 0.15	$M_{\text{NFW}}, T > 3.5$ keV
FRB01	3.26 ± 0.60^c	1.48 ± 0.11	$M_{\beta\gamma}, T > 3$ keV
FRB01	3.31 ± 0.45^c	1.78 ± 0.10	$M_{\beta\gamma}, T > 0.9$ keV
<u>Theory</u>			
EMN96	5.6	1.5	T_{ew} , adiabatic simul.
VBB02	3.6	~ 1.7	T_{em}
BMS04	4.6 ± 0.2	1.59 ± 0.05	$T_{\text{em}}, T > 0.7$ keV
RMB05	7.2 ± 0.5	1.66 ± 0.09	$T_{\text{sl}}, T > 1$ keV
RMB05	4.2 ± 0.2	1.53 ± 0.05	$M_{\beta\gamma}, T_{\text{sl}}, T > 1$ keV
$\delta = 200$			
<u>Observation</u>			
Present work	5.34 ± 0.22	1.72 ± 0.10	$M_{\text{NFW}}, T > 2$ keV
Present work	5.74 ± 0.30	1.49 ± 0.17	$M_{\text{NFW}}, T > 3.5$ keV
SPF03	4.5 ± 0.3^c	1.84 ± 0.06	$M_{\beta\gamma}, T > 0.6$ keV
<u>Theory</u>			
EMN96	7.4	1.5	T_{em} , adiabatic simul.
MTK02	7.6	1.61	$T_{\text{em}}, T > 2.0$ keV

Notes: (a): References: (ASF01) Allen et al. (2001); (BMS04) Borgani et al. (2004); (EMN96) Evrard et al. (1996); (FRB01) Finoguenov et al. (2001); (KSA04) Kay et al. (2004b); (MTK02) Muanwong et al. (2002); (PW) present work; (RMB05) Rasia et al. (2005); (SPF03) Sanderson et al. (2003); (VBB02) Voit et al. (2002); (b): Method: (M_{NFW}): mass estimated using an NFW model to describe the mass profile; ($M_{\beta\gamma}$): mass estimated using a polytropic β -model for the gas distribution; (T_{m}): mass-weighted temperature; (T_{em}): emission-weighted temperature; (T_{sl}): spectroscopic-like temperature as defined in Mazzotta et al. (2004). (c): The normalisation at 5 keV is derived from the published normalisation at 1 keV and the best fitting slope. The fractional error has been assumed to be the same, which is conservative.

5. Comparison with previous observations

In the present study, as discussed above, an NFW profile has been used to describe the integrated mass profile, derived, assuming HE, from the observed density and temperature profiles. A similar approach⁴ was used in the *Chandra*

⁴ The method slightly differs from ours. Allen et al. (2001) predict the temperature profile corresponding to a given NFW mass profile

study of Allen et al. (2001). Previous *ROSAT/ASCA* studies also estimated the mass from the HE equation, but assumed a β -model for the gas density profile and a polytropic (or even isothermal) temperature profile (Horner et al. 1999; Nevalainen et al. 2000; Finoguenov et al. 2001; Xu et al. 2001; Castillo-Morales & Schindler 2003; Sanderson et al. 2003). Data were of poorer spatial resolution and statistical quality, and extended to lower radii, thus requiring more extrapolation, particularly for low mass clusters. This could introduce systematic errors and biases, particularly at low δ , since a mass profile derived from an isothermal or polytropic β -model is not consistent with an NFW profile at large radii (see Fig 11 of Neumann & Arnaud 1999). On the other hand, the latest *ROSAT/ASCA* studies of the $M-T$ relation (Finoguenov et al. 2001; Sanderson et al. 2003) are superior in terms of the size of the cluster samples, and their wide and homogeneous coverage in temperature. Their results are compared to ours in Table 3.

Finoguenov et al. (2001) established the $M_{500}-T$ relation for 39 clusters with *ASCA* temperature profiles. Interestingly, their results are consistent with ours within the uncertainties (Table 3). This suggests that systematic errors are not dominant over statistical errors at $\delta = 500$ in this *ROSAT/ASCA* study. However, our normalisation is on the upper side of their allowed values. The slope they find for their hot cluster subsample ($T > 3$ keV) is, as we have found, consistent with the expected $\alpha = 1.5$ value. When Finoguenov et al. (2001) included all clusters (down to $T \sim 0.9$ keV), they found a steepening of the $M_{500}-T$ relation: $\alpha = 1.78 \pm 0.1$. The effect is larger than in our case: we find $\alpha = 1.71 \pm 0.09$ (although the difference is not significant). However, our sample does not reach quite such low temperatures and the difference could also reflect a progressive steepening of the $M-T$ relation toward low masses.

The same remark holds for the results of Sanderson et al. (2003), who derived a slope of $\alpha = 1.84 \pm 0.06$ for the $M_{200}-T$ relation, which is barely consistent with our value. Their large sample includes 66 clusters in the [0.5 – 15] keV temperature range. However, their normalisation is significantly (by 15%, Table 3) lower than ours. This may reflect systematic errors introduced when extrapolating polytropic models down to δ as low as 200. However, such systematic errors could not explain the discrepancy between our results and theirs at $\delta = 2500$. At that density contrast, they still find a slope of $\alpha = 1.84 \pm 0.14$ for hot clusters ($T > 5.5$ keV), a result inconsistent with ours at the $\sim 95\%$ confidence level. They also derive a lower normalisation: $(1.2 \pm 0.4) \times 10^{14} M_{\odot}$ compared to $(1.69 \pm 0.05) \times 10^{14} M_{\odot}$. Their normalisation was only barely consistent with *Chandra* results.

Sanderson et al. (2003) have suggested that the discrepancy might be related to the dynamical state of the clusters in the different samples. Both the *Chandra* study and the present *XMM-Newton* study focus on particularly relaxed clusters, which is not the case in Sanderson et al.'s study. However, we note that Finoguenov et al.'s sample does not discriminate in terms of dynamical state, and their results are in good agree-

and the observed surface brightness profile and fit it to the observed temperature profile.

ment with ours. That said, the $M-T$ relation could well depend on the exact dynamical states of the clusters in the sample in question, an effect which is not trivial to predict. The numerical simulations of Rowley et al. (2004) show (their Fig. 15) that clusters with substructure tend to lie below the mean $T-M$ relation, probably due to incomplete thermalisation. However, for the same reason, we would expect the X-ray mass to underestimate the true mass (Kay et al. 2004a), moving unrelaxed clusters back closer to the mean relation. A *XMM-Newton* study of the $M-T$ relation for an unbiased sample of clusters is needed to assess the effect of cluster dynamical state on the measured $M-T$ relation. The relation should ideally be compared to numerical simulations and lensing mass data. In any case, we do not confirm the Sanderson et al. (2003)'s results, at least for relaxed clusters considered here.

Finally, it is of interest to compare the present results with those of Ettori et al. (2002), who also use an NFW model to estimate masses⁵. Their $M-T$ relation for 12 Cooling Flow clusters (relaxed clusters) with $T > 3$ keV can be directly compared with our relation for hot clusters. At $\delta = 2500$, they found $\alpha = 1.88 \pm 0.27$, which is marginally consistent with our value, and $\alpha = 2.3 \pm 0.4$ at $\delta = 500$, a value clearly rejected by our data. However, their $M-T$ relation already has a large scatter at $\delta = 2500$, which becomes dramatic at $\delta = 500$ (their Figure 5). We do not observe such a scatter. It may reflect systematic errors connected to the extrapolation of the NFW model. As we discussed above in Sect. 3.2, the precision on extrapolated mass depends on the precision on the concentration parameter, which is more difficult to constrain with *BeppoSAX* than with *XMM-Newton*.

6. Comparison with theoretical predictions

The ICM temperature structure in a cluster is the result of the complex interplay between gravitational processes (i.e., the evolution of the gas in the Dark Matter potential), and of any other process that can affect the gas entropy (e.g., cooling and heating from galaxy feedback). The theoretical $M-T$ relation – which should be viewed rather as a T versus M relation when predicted from theoretical studies – depends on the exact modelling of all these processes. Moreover, as we discuss below, comparison of observations and theory also depends on the exact definition of the 'average' temperature, since the gas is never perfectly isothermal.

6.1. The normalisation of the $M_{\delta}-T$ relation at 5 keV

The normalisation of the $M-T$ relation is particularly well constrained by our study, the statistical error being now less than $\sim 5\%$ at 5 keV. The value of the normalisation depends on the (sub)sample considered because it is correlated with the slope. However by choosing a reference temperature of 5 keV, close to the median temperature, we minimize the effect, and the difference is of the order of the statistical error. We can thus first

⁵ In their approach, the predicted temperature profile was fitted to the observed *BeppoSAX* temperature profile.

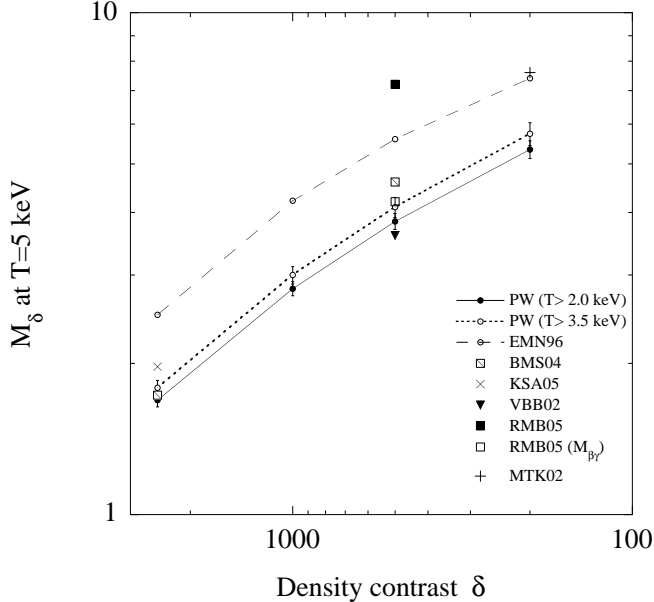


Fig. 4. The normalisation of the M_δ - T relation at $T = 5$ keV for various δ . The results of theoretical works (see Table 3 for references) are compared to the values derived in the present work (PW).

compare our results with the predicted values, quasi- independently of the slope issue.

6.1.1. Adiabatic models

The difference with the prediction from adiabatic models is not dramatic, particularly when the dispersion among various adiabatic simulations is taken into account. The normalisation is 30% below the prediction of Evrard et al. (1996), compared to typically more than 50% difference in the normalisation derived from different adiabatic simulations (Henry 2004, Table 3). However, as discussed by Muanwong et al. (2002), higher resolution simulations tend to predict higher normalisation, thus exacerbating the discrepancy with our results. Adiabatic simulations probably fundamentally fail to predict the correct normalisation of the M - T relation. The observed discrepancy could in principle be due to incorrect modelling of the Dark Matter component itself, since it is this which drives the potential. We have already argued that this is not the case from the excellent agreement between the observed and simulated mass profiles (Paper I and Sec. 4). A more likely explanation is that non-gravitational processes affect the M - T relation, as they affect all other relations.

6.1.2. Non-adiabatic models

From theoretical arguments and from observations of the gas entropy, it is clear now that both cooling and galaxy feedback have to be taken into account when discussing relations involving the ICM (Voit & Ponman 2003; Pratt & Arnaud 2005). We thus focus on published theoretical studies that include both

phenomena. Their predictions are compared with our results in Table 3 and in Fig. 4. All of the quoted simulations are made in the 'concordance' Λ CDM cosmology, and use the same definition of M_δ as in the present work. However, they are not always using the same definition of the temperature (see below).

As a given mass, cooling and galaxy feedback increase the gas entropy as compared to the value attained by pure gravitational heating. This increases the temperature and, as expected, a lower normalisation is found when these processes are included in a given numerical simulation (Muanwong et al. 2002; Thomas et al. 2002) or analytical model (Voit et al. 2002). Recent non-adiabatic simulations seem to be quite successful at reproducing the observed M_{2500} - T relation. The normalisation derived by Borgani et al. (2004), for a sample of simulated clusters with temperatures $T > 2$ keV, is in perfect agreement with our value (see also Fig. 3), while the normalisation derived by Kay et al. (2004b, see also Thomas et al. (2002)) is only $\sim 10\%$ too high. These works used the mass weighted temperature, $T_{m,2500}$, estimated within R_{2500} , which is directly linked to the thermal energy. As discussed in Sect. 2.2 our spectroscopic temperature, T_s , should be close to the mass weighted temperature in that region. Thus, the good agreement between the observed M_{2500} - T_s and predicted M_{2500} - T_m relations is encouraging, and suggests that the thermal energy content in this central region is roughly correctly modelled.

Up until recently, the standard temperature definition used to mimic X-ray observations in numerical simulation studies was the emission-weighted temperature T_{em} . Using this temperature definition at $\delta = 500$, the normalisation of Borgani et al. (2004) is now too high by about 12 – 20%, the normalisation found by Voit et al. (2002) is marginally too low and the normalisation found by Muanwong et al. (2002) at $\delta = 200$ is 30% too high (Fig. 4). It is likely that the variability of these results is linked to differences in the various physical models used.

Independent of the physics, a crucial point seems to be the exact definition of the temperature. Recently, Mazzotta et al. (2004) introduced the spectroscopic-like temperature (T_{sl}) in order to better reproduce the temperature obtained from spectral fits when the ICM is multi-temperature. Mazzotta et al. show that T_{sl} is biased towards the lower values of the dominant thermal component, and that in general T_{em} overestimates T_{sl} . Unfortunately, this exacerbates the disagreement between observed and simulated M_{500} - T normalisations. Using T_{sl} , Rasia et al. (2005) over-predict a normalisation, relative to our values, by a factor as large as ~ 1.8 . Note that Rasia et al. use the same physical model as Borgani et al. (2004) and yet their normalisation is $\sim 50\%$ higher (see Table 3 and also their Fig 2). Strictly speaking these temperatures were estimated with R_{500} , whereas our spectroscopic temperature measurement T_s is interior to $0.5R_{200}(\sim R_{1000})$. A1413 is the only cluster for which we have data up to $\delta = 500$. The spectroscopic temperature within $\delta = 500$, $T_{s,500}$ is only slightly smaller (by 3%) than T_s . This would increase the normalisation of the M_{500} - T relation by less than 5% if we used $T_{s,500}$ (assuming the same correction factor for all clusters).

It thus appears that there is a genuine disagreement between observed and predicted normalisation of the M_{500} - T re-

lation. One interpretation, as proposed by Rasia et al. (2005), is that the X-ray mass underestimates the 'true' mass (see also Borgani et al. 2004; Muanwong et al. 2002). Using T_{sl} temperatures, they estimated the value of M_{500} that an X-ray observer would derive from their simulation using the HE equation and a polytropic β -model. The resulting $M_{500} - T_{\text{sl}}$ is indeed now in good agreement with our observation (Table 3 and Fig. 4). However, the normalisation is $4.2 \pm 0.2 \times 10^{14} M_{\odot}$, as compared to $7.2 \pm 0.5 \times 10^{14} M_{\odot}$ when using the 'true' theoretical mass. This corresponds to a very serious underestimate of the mass by X-ray observations: the 'true' M_{500} mass of clusters would be a factor $\sim 7.2/4.2 = 1.7$ higher than the X-ray mass. We think this is very unlikely, at least for the masses estimated as in the present work. Firstly, our approach, fitting an NFW model and extrapolating the mass profiles, is more sophisticated than the simple polytropic β -model approach. Secondly, we note again the excellent quantitative agreement of our mass profiles with theoretical predictions. If we have underestimated the 'true' M_{500} by a factor 1.7, we should also have underestimated the 'true' M_{2500} by the same factor. This is ruled out from combined lensing/X-ray studies: Allen et al. (2001) conclude that systematic uncertainties are less than 20%⁶. Conversely, for the X-ray mass profiles to have the correct universal shape, as we have observed, the predicted difference between the X-ray mass estimates and the true mass should be roughly constant with radius. This is not what is expected if the difference is important at $\delta = 500$: it is linked to differences between the temperature profile derived from projected $T_{\text{sl}}(r)$ values and the true profile, which depends on the ICM structure along the line of sight (Mazzotta et al. 2004; Rasia et al. 2005), and thus *a priori* on radius. It would be interesting to check this point with numerical simulations.

A more likely explanation is that numerical simulations do not correctly describe the gas thermal structure at large scale, at least for relaxed clusters considered here. We note that numerical simulations predict temperature profiles decreasing with radius, by nearly a factor 2 at $\delta = 500$ (Borgani et al. 2004, Fig 6), while the observed profile is flatter (Fig. 1). This would bias low the T_{sl} as compared to the X-ray temperature of real clusters, and thus increase the normalisation of the $M_{500}-T_{\text{sl}}$ relation⁷. It would be interesting to compare the theoretical $M_{2500}-T_{\text{sl}}$ and $M_{2500}-T_{\text{m}}$ relations, and investigate if there is a continued good agreement with observations. We expect this to be the case since the predicted temperature variations are not dramatic - less than 20% variations within $\delta = 2500$ (see Fig 6 of Borgani et al. (2004) and Fig 9 of Kay et al. (2004a)), so that T_{sl} should be close to T_{m} .

6.2. The slope of the $M-T$ relation

The observed $M-T$ relation slope is consistent with the self-similar expectation for the sub-sample of hot clusters ($T >$

⁶ Note that our $M_{2500}-T$ relation is the same than found by Allen et al. (2001).

⁷ Since T_{em} is less affected, the predicted $M_{500}-T_{\text{em}}$ relations would be in better agreement with observations.

3.5 keV): $\alpha = 1.51 \pm 0.11$ at $\delta = 2500$, where it is best constrained. The slope is significantly higher when the whole sample ($T > 2$ keV) is considered: $\alpha = 1.71 \pm 0.07$.

A value of $\alpha = 1.5$ is expected from the virial theorem if clusters obey self-similarity. All adiabatic simulations confirm this value (Evrard et al. 1996; Pen 1998; Eke et al. 1998; Bryan & Norman 1998; Yoshikawa et al. 2000; Thomas et al. 2001), including when a wide bandpass spectral temperature, as measured with *Chandra* or *XMM-Newton*, is used to establish the $M-T$ relation (Mathiesen & Evrard 2001). Numerical simulations including cooling and feedback do predict a slightly higher slope. However, the effect is smaller than we observe ($\Delta(\alpha) = 0.05 - 0.1$) and is generally not significant (Table 3). The only exception is the $M_{500}-T_{\text{sl}}$ relation derived by Rasia et al. (2005): $\alpha = 1.66 \pm 0.09$. However the normalisation is then much too high (see above). It is also worth noting that the phenomenological analytical model of Voit et al. (2002) yields a larger slope. We obtained $\alpha \sim 1.7$ by fitting their relation (their Fig 22) in our temperature range. This is in good agreement with the observed value; however, in this case the larger slope is mostly due to the variation of the concentration of the Dark Matter with mass in their model (Voit et al. 2002), which is larger than we observe (Paper I).

As a final remark, we want to emphasise that the observed discrepancy with the standard self-similar value is actually small. The slope increase, observed when including cool clusters, is significant at most at the $\sim 85\%$ confidence level. Furthermore, at 2 keV, the limiting temperature of our sample, this corresponds to only $\sim 20\%$ difference in mass as compared to the extrapolation of the best fitting $M-T$ relation for hotter clusters (see also Fig. 3). There is scatter in the $M-T$ relation, and our sample comprises only 4 cool clusters. We thus cannot exclude that the steepening is an artefact of our particular choice of clusters. We also note that the quality of the power law fit decreases when including low mass systems. This may indicate that the $M-T$ relation is actually convex in the log-log plane, either across the entire temperature range, or below a 'break' temperature. We lack clusters in the intermediate temperature range to assess this issue. Clearly, a possible discrepancy between predicted and observed slopes needs to be confirmed and better specified by considering a larger cluster sample.

7. Conclusion

Using a sample of ten relaxed galaxy clusters observed with *XMM-Newton*, we have calibrated the local $M_{\delta}-T$ relation, in the temperature range [2 – 9] keV, at four density contrasts, $\delta = 2500, 1000, 500, 200$. We used the spectroscopic temperature estimated within $0.5R_{200}$ ($\delta \sim 1000$), excluding the cooling core region, and the masses at various δ are derived from NFW profile fits to precise mass profiles measured up to at least $\delta = 1000$. We argue that our measured masses are particularly reliable. The logarithmic slope of the $M_{\delta}-T$ relation is the same at all δ , reflecting the self-similarity of the mass profiles. The slope is well constrained and is consistent with the standard self-similar expectation, $\alpha = 1.5$, for the sub-sample of hot clusters ($T > 3.5$ keV). The relation steepens to $\alpha \sim 1.7$ when

the whole sample ($T > 2$ keV) is considered. The normalisation of the $M-T$ relation is measured with a precision better than $\pm 5\%$ and is 30% below the value predicted by the adiabatic numerical simulations of Evrard et al. (1996).

Models that take into account radiative cooling and galaxy feedback are now in good agreement with the observed $M_{2500} - T$ relation. We argue that remaining discrepancies at $\delta = 500$ and lower are more likely to be due deficiencies in models of the ICM thermal structure, to which the spectroscopic-like temperature seems to be very sensitive, rather than to an incorrect estimate of the mass from X-ray data.

More detailed comparisons are needed to understand the origin of the discrepancies between the predicted and observed $M-T$ relations. Our directly measured $M_{1000} - T$ relation now provides the most direct constraint at large scale for numerical simulations. Simulations of mass profiles, as would be determined by an X-ray observer using modern *Chandra* and *XMM-Newton* techniques, are also needed. This would be particularly interesting for relaxed cluster sub-samples, and using better representations of observed temperatures (e.g. as proposed by Mazzotta et al. (2004)). Such data could be directly compared to observed mass profiles. This would provide information on i) possible overall systematic errors in X-ray mass estimates, and ii) further test the reliability of simulations to correctly reproduce the ICM structure.

On the observational side, study of a much larger, unbiased, sample is needed to i) determine the exact shape of the local $M-T$ relation; ii) study its intrinsic scatter, and iii) assess the effect of cluster dynamical state on the $M-T$ relation.

Acknowledgements. The present work is based on observations obtained with *XMM-Newton* an ESA science mission with instruments and contributions directly funded by ESA Member States and the USA (NASA). EP acknowledges the financial support of CNES (the French space agency). GWP acknowledges funding from a Marie Curie Intra-European Fellowship under the FP6 programme (Contract No. MEIF-CT-2003-500915).

References

Allen, S. W., Schmidt, R. W., & Fabian, A. C. 2001, MNRAS, 328, L37

Bertschinger, E. 1998, Ann. Rev. Astron. Ap., 36, 599

Borgani, S., 2003, in "The Riddle of Cooling Flows in Galaxies and Clusters of galaxies", Eds. T. Reiprich, J. Kempner, and N. Soker, <http://www.astro.virginia.edu/coolflow/>

Borgani, S., Murante, G., Springel, V., et al. 2004, MNRAS, 348, 1078

Bryan, G. L. & Norman, M. L. 1998, ApJ, 495, 80

Castillo-Morales, A. & Schindler, S. 2003, A&A, 403, 433

Ettori, S., De Grandi, S., & Molendi, S. 2002, A&A, 391, 841

Evrard, A. E., Metzler, C. A., & Navarro, J. F. 1996, ApJ, 469, 494

Evrard, A.E., & Gioia, I. 2002, in Merging Processes in Galaxy Clusters, ed. L. Feretti, I.M. Gioia, G. Giovannini, Astrophysics and Space Science Library, Vol. 272, 253

Finoguenov, A., Reiprich, T. H., & Böhringer, H. 2001, A&A, 368, 749

Eke, V.R., Navarro, J.F., & Frenk, C. S. 1998, ApJ, 503, 569

Henry, J.P., 2004, ApJ, 609, 603

Horner, D. J., Mushotzky, R. F., & Scharf, C. A. 1999, ApJ, 520, 78

Kay, S. T., Thomas, P. A., Jenkins, A., & Pearce, F. R. 2004a, MNRAS, 355, 1091

Kay, S. T., Thomas, P. A., Jenkins, A., & Pearce, F. R. 2004b, astro-ph/0411650

Mathiesen, B. F. & Evrard, A. E. 2001, ApJ, 546, 100

Mazzotta, P., Rasia, E., Moscardini, L., & Tormen, G. 2004, MNRAS, 354, 10

Muanwong, O., Thomas, P. A., Kay, S. T., & Pearce, F. R. 2002, MNRAS, 336, 527

Navarro, J. F., Frenk, C. S., & White, S. D. M. 1997, ApJ, 490, 493

Neumann, D. M. & Arnaud, M., 1999, A&A, 348, 711

Nevalainen, J., Markevitch, M., & Forman, W. 2000, ApJ, 532, 694

Pen, U. L. 1998, ApJ, 498, 60

Pierpaoli, E., Borgani, S., Scott, D., & White, M., 2003, MNRAS, 342, 163

Pointecouteau, E., Arnaud, M., Kaastra, J., & de Plaa, J. 2004, A&A, 423, 33

Pointecouteau, E., Arnaud, M. & Pratt, G.W., 2005, A&A, in press (astro-ph/0501635)

Pratt, G. W. & Arnaud, M. 2002, A&A, 394, 375

Pratt, G. W. & Arnaud, M. 2005, A&A, 429, 791

Rasia, E., Tormen, G., & Moscardini, L., 2004, MNRAS, 351, 237

Rasia, E., Mazzotta, P., Borgani, S., et al. 2005, ApJ, 618, L1

Rowley, D. R., Thomas, P. A., & Kay, S. T. 2004, MNRAS, 352, 508

Sanderson, A. J. R., Ponman, T. J., Finoguenov, A., Lloyd-Davies, E. J., & Markevitch, M. 2003, MNRAS, 340, 989

Thomas, P. A., Muanwong, O., Kay, S. T., Pearce, F. R., Couchman, H.M.P., Edge, A.C., Jenkins A., & Onuora L., 2001, MNRAS, 324, 450

Thomas, P. A., Muanwong, O., Kay, S. T., & Liddle, A.R., 2002, MNRAS, 330, L48

Viana, P., Kay, S.T., Liddle, A.R., Muanwong, O., & Thomas, P.A., 2003, MNRAS, 346, 319

Voit, G.M., Bryan, G.L., Balogh, M.L., & Bower, R.G. 2002, ApJ, 576, 601

Voit, G.M., Ponman, T.J., 2003, ApJ, 594, L75

Xu, H., Jin, G., & Wu, X. P. 2001, ApJ, 553, 78

Yoshikawa, K., Jing, Y.P., & Suto, Y., 2000, ApJ, 535, 593